Journal of Materials Chemistry A

RSC Publishing

PAPER

View Article Online
View Journal | View Issue

Cite this: J. Mater. Chem. A, 2013, 1, 9107

Self-assembling hybrid NiO/Co_3O_4 ultrathin and mesoporous nanosheets into flower-like architectures for pseudocapacitance†

Kaibing Xu, Rujia Zou, Wenyao Li, Yafang Xue, Guosheng Song, Qian Liu, Xijian Liu and Junqing Hu*

Received 18th March 2013
Accepted 17th May 2013

DOI: 10.1039/c3ta11099k

www.rsc.org/MaterialsA

The rational design and synthesis of mesoporous hybrid architecture electrode materials for high-performance pseudocapacitor applications still remains a challenge. Herein, we demonstrate the design and fabrication of hybrid NiO/Co_3O_4 flower-like mesoporous architectures on a large-scale for high-performance supercapacitors by a facile, environmentally friendly, and low-cost synthetic method. The as-synthesized hybrid NiO/Co_3O_4 flower-like architectures show a high specific capacitance of 1068 F g^{-1} at a scan rate of 5 mV s^{-1} and 1190 F g^{-1} at a current density of 4 A g^{-1}, a good rate capability even at high current densities and an excellent long-term cycling stability (less than 1% loss of the maximum specific capacitance after 5000 cycles), which can be mainly attributed to their morphological characteristics of mesoporous and ultrathin nanosheets self-assembling into flower-like architectures, as well as a rational composition of the two constituents. The remarkable electrochemical properties, as well as many advantages associated with the synthetic method, should make the present architectures competitive electrode materials for next generation supercapacitors.

1 Introduction

Because of their remarkable chemical and physical properties, three dimensional (3D) microstructures formed by the assembly of one dimensional (1D) (such as nanowires or nanotubes) or two dimensional (2D) (such as nanosheets or nanoflakes) nanostructures are expected to provide solutions to the practical needs of energy-storage devices,[1] nanophotonics,[2] bionanotechnology,[3] and catalysis.[4] Supercapacitors, which are also known as electrochemical capacitors and are divided into electrical double-layer capacitors and pseudocapacitors according to the charge-storage mechanism, have drawn worldwide research attention as the most promising candidates for next-generation high-capacitance energy storage devices.[5] Until now, the major classes of materials, including carbonaceous materials,[6] transition-metal oxides (TMOs, such as RuO_2,[7] NiO,[8] Co_3O_4,[9] MnO_2,[10] and VO_x,[11] *etc.*) and conducting polymers,[12] have been studied as electrode materials for the supercapacitors. Among them, the TMOs can store charges with surface Faradaic (redox) reactions, which enable a higher energy density compared with the other two materials, and thus are considered as ideal electrode materials for the pseudocapacitors. Though RuO_2 is reported to have the most promising performances, offering a high specific capacitance with excellent cyclability, its expensive and toxic nature limits its large-scale commercial application,[13] and other inexpensive and environmentally friendly TMOs have been developed as alternatives. Among these candidates, NiO and Co_3O_4 have received tremendous interest recently in supercapacitor applications due to their controllable size and morphology, tunable surface and structural properties, high theoretical capacity (2584 F g^{-1} and 3560 F g^{-1}, respectively), good electronic conductivity, favorable capacitive characteristics, and good corrosion stability in alkaline solutions.[14] Many reports are available on the synthesis and electrochemical properties of 1D, 2D and 3D nano/microstructures from NiO and Co_3O_4 materials. Zhang *et al.* reported a specific capacitance of 525 F g^{-1} for NiO nano/microspheres as an electrode material at a current density of 4 A g^{-1} *via* a refluxing approach.[15] Rao *et al.* fabricated layered Co_3O_4 microstructures with a high specific capacitance of 548 F g^{-1} at a current density of 8 A g^{-1}.[16] Unfortunately, in these cases the observed specific capacitances are still far below the theoretical values, especially at high rates.

Recently, much attention has been focused on improving the specific capacitance of supercapacitors, by exploring novel materials with the rational design of multi-component combination, which can provide the synergistic effect of all individual constituents, as well as controllable 3D hierarchical heterostructures, which can provide efficient and rapid pathways for ion and electron transport, not only at their surfaces, but

State Key Laboratory for Modification of Chemical Fibers and Polymer Materials, College of Materials Science and Engineering, Donghua University, Shanghai 201620, China. E-mail: hu.junqing@dhu.edu.cn

† Electronic supplementary information (ESI) available: Supplementary figures. See DOI: 10.1039/c3ta11099k

throughout the bulk of the chemical distributions.[17] Fan *et al.* reported Co_3O_4/NiO core/shell nanowire arrays on a Ni foam substrate by hydrothermal and chemical bath deposition methods as an electrode material, which showed a specific capacitance of 853 F g^{-1} at 2 A g^{-1} and good cycling stability.[18] Also, CoO@$Ni(OH)_2$ hybrid nanostructures on Ni foam have been fabricated by the electrodeposition process for pseudocapacitors, which have a high area capacitance up to 11.5 F cm^{-2}.[19] Tong *et al.* reported Co_3O_4/$Ni(OH)_2$ composite mesoporous nanosheets on Ti substrates *via* an electrochemical deposition route as an electrode material, which showed a high specific capacitance of 1144 F g^{-1} at 5 mV s^{-1} and long-term cyclability.[20] Although better electrochemical properties have been achieved, the fabrication processes involving substrate materials and deposition growth are complicated, time-consuming, and have low repeatability, and particularly, as-synthesized products have a low yield, thus hindering their widely commercial applications in an energy storage system. It is thus of great interest to design hybrid architectures with excellent electrochemical properties and to develop a facile, environmentally friendly, low-cost, and large-scale synthetic method for supercapacitor applications.

Herein, we demonstrate the design and synthesis of mesoporous hybrid NiO/Co_3O_4 flower-like architectures on a large scale *via* a facile solvothermal route for supercapacitor applications. These flower-like architectures are 3D self-assembled by NiO/Co_3O_4 ultrathin and mesoporous sheets, and not only provide a high active surface area and a large inner space but also have a strong synergistic effect from NiO and Co_3O_4, thus leading to excellent electrochemical properties. As an electrode material for pseudocapacitors, the hybrid NiO/Co_3O_4 flower-like architectures show a specific capacitance of 1190 F g^{-1} and a very long-term cycling stability (less than 1% loss of the specific capacitance after 5000 cycles), which are both significantly improved, as compared with as-synthesized NiO flower-like architectures (960 F g^{-1} and less than 5% loss after 5000 cycles). These hybrid NiO/Co_3O_4 flower-like architectures showing high-performance capacitive behavior through an environmentally friendly, low-cost, and large-scale synthetic method will be a promising electrode material for fabricating supercapacitors.

2 Experimental section

2.1 Materials preparation

All the reagents used were of analytical grade (purchased from Sinopharm) and used without further purification. Here, two kinds of hybrid NiO/Co_3O_4 flower-like architectures and NiO flower-like architectures were synthesized through combining a solvothermal reaction and thermal annealing process. In a typical synthetic procedure, taking NiO flower-like architectures as an example, $Ni(NO_3)_2 \cdot 6H_2O$ (3.4 mmol) and polyvinylpyrrolidone (PVP) (0.5 g) were dissolved in deionized water (5 mL) and absolute methanol (43 mL) under vigorous magnetic stirring. After stirring for 1 h, the as-obtained solution was transferred into a 60 mL polytetrafluoroethylene (PTFE) (Teflon)-lined autoclave and maintained at 180 °C for 6 h in an electric oven. After being cooled to room temperature naturally, the precipitate was collected and washed with deionized water and ethanol several times by centrifugation, then dried at 60 °C overnight. Afterwards, the samples were calcined at 450 °C for 40 min at a ramping rate of 1 °C min^{-1} to transform into NiO. In the cases of the hybrid materials, two kinds of NiO/Co_3O_4 flower-like architectures were synthesized by the same procedure as described above, except that the cobalt source ($Co(NO_3)_2 \cdot 6H_2O$) with various mole ratios (4 : 1 and 3 : 2) of $Ni(NO_3)_2$ to $Co(NO_3)_2$ was added to the starting materials with a total concentration of the two metal salts of 3.4 mmol.

2.2 Materials characterization

The as-synthesized products were characterized with a D/max-2550 PC X-ray diffractometer (XRD; Rigaku, Cu-Kα radiation), a scanning electron microscope (SEM; S-4800), a transmission electron microscope (TEM; JEM-2100F) equipped with an energy dispersive X-ray spectrometer (EDX), and an X-ray photoelectron spectrometer (ESCALab MKII) with an excitation source of Mg-Kα radiation. The surface area, pore size, and pore-size distribution of the products were determined by Brunauer–Emmett–Teller (BET) nitrogen adsorption–desorption and Barrett–Joyner–Halenda (BJH) methods (Micromeritics, ASAP2020).

2.3 Electrochemical measurement

The electrochemical performances of the as-synthesized active materials were investigated on an Autolab (PGSTAT302N potentiostat) using a three-electrode mode in 1 M KOH solution. Working electrodes were prepared by mixing each as-synthesized active material (80 wt%) with acetylene black (15 wt%) and polyvinylidene fluoride (PVDF, 5 wt%) in NMP (*N*-methyl-2-pyrrolidone). A small amount of absolute ethanol was then added to the mixture to promote homogeneity, followed by 24 h of stirring. The as-obtained mixture was then pressed onto the Ni foam substrate and dried at 120 °C for 4 h to remove the solvent. After that, the as-formed electrodes were pressed at 10 MPa. The loading mass was about 1.9, 0.8, and 0.7 mg for NiO, NiO/Co_3O_4(4 : 1), and NiO/Co_3O_4(3 : 2), respectively. The reference electrode and counter electrode were Ag/AgCl and platinum, respectively.

3 Results and discussion

The hybrid NiO/Co_3O_4 and NiO flower-like architectures were prepared by a simple solvothermal route (using $Ni(NO_3)_2$ and $Co(NO_3)_2$ as source materials) followed by a thermal annealing at 450 °C (see the Experimental section for the details). For a comparison, as-synthesized NiO products were first characterized, Fig. 1 (the yield of the NiO products was up to ~20% (theoretical value: 25.39%), according to the amount of $Ni(NO_3)_2$ used. Fig. S1† shows a large-scale photograph of the as-synthesized hybrid NiO/Co_3O_4 flower-like architectures). As seen from a low-magnification SEM image, Fig. 1a, the as-synthesized NiO products consisted of a large quantity of spherically shaped architectures, appearing like *Ranunculus asiaticus* flowers with a fairly uniform diameter of ~1 μm (an

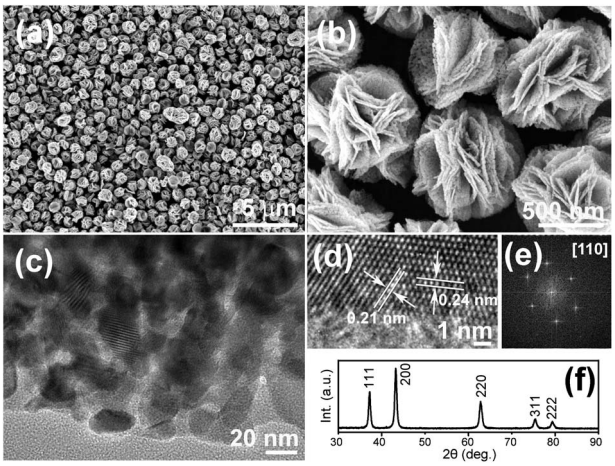

Fig. 1 (a and b) Low- and high-magnification SEM images of the as-synthesized NiO flowers. (c) TEM image of a NiO sheet with a densely mesoporous nature. (d and e) HRTEM image of the NiO sheet and corresponding FFT pattern, respectively. (f) XRD pattern of the as-synthesized NiO material.

upper-right inset). In fact, each "flower" is composed of many mesoporous and very thin sheets (~5 to 10 nm in thickness), Fig. 1b. Compared with the solvothermal products (or intermediates), it was found that the product morphology undergoes a significant change from buds (Fig. S2†) to blooming flowers after such an annealing process. A high-magnification TEM image, Fig. 1c, further demonstrates that each NiO sheet is full of numerous pores with diameters of ~10 to 20 nm (or Fig. S2d†), which is due to the fact that the surfactant, H_2O, and gases are released and lost during the intermediates' decomposition/oxidation through this thermal annealing. Fig. 1d is a high-resolution TEM image (HRTEM) of the NiO nanosheet as in (c). The lattice fringes show the imaging characteristics of the cubic NiO crystal, in which the *d*-spacing of 0.24 and 0.21 nm corresponds to the distance of the $\{1\bar{1}1\}$ and $\{002\}$ planes, respectively, of the NiO crystal; an inset fast Fourier transformation (FFT) pattern from this image can be indexed as the [110] zone axis of the NiO crystal. In our study, we have carefully examined a large area of this sheet by HRTEM imaging without any tilting of the sample. All the images taken exactly demonstrated the same lattice fringe characteristics of the NiO crystal without an orientation variation. This indicates the NiO sheet is a single-crystal in nature, but full of numerous nanopores. An X-ray diffraction (XRD) pattern, Fig. 1f, reveals the overall crystal structure and phase purity of the products. All the diffraction peaks can be indexed to the cubic phase NiO with lattice constants of $a = 4.18$ Å, in agreement with the reported values from the JCPDS card (04-0835). These results illustrate that the as-prepared products were indeed composed of the cubic phase NiO material.

Hybrid NiO/Co_3O_4 materials were prepared by adding cobalt source into the starting materials with various mole ratios of $Ni(NO_3)_2$ to $Co(NO_3)_2$. The products shown in Fig. 2 were synthesized by using the mole ratio of 4 : 1 and keeping the other synthetic conditions constant. As seen from a low-magnification SEM image, Fig. 2a, the products still consisted

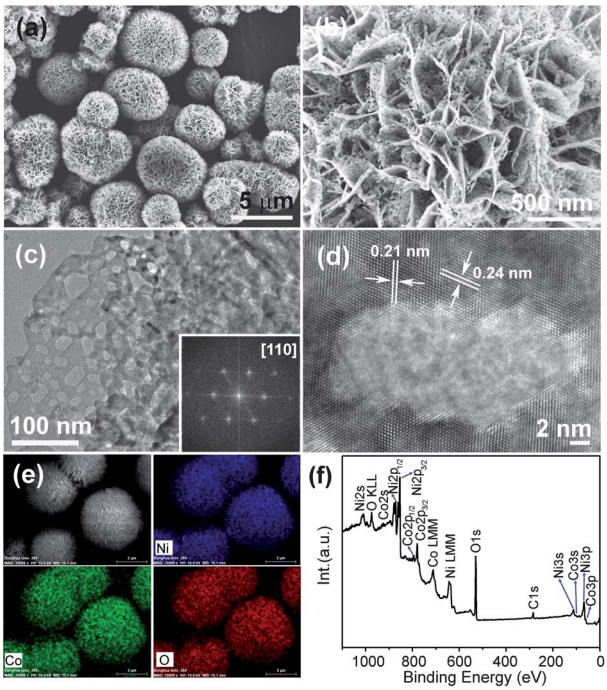

Fig. 2 (a and b) Low- and high-magnification SEM images of the as-synthesized hybrid NiO/Co_3O_4 (4 : 1) materials. (c and d) TEM and HRTEM images of an individual sheet, the inset in (c) shows its corresponding FFT pattern. (e) EDX elemental mappings and (f) XPS survey scan of the NiO/Co_3O_4 (4 : 1) flower-like architectures.

of a lot of spherical flower-like architectures, a few of which displayed a twin-sphere shape for a flower-like structure. However, compared with the former NiO flower-like architectures, their mean sizes were not uniform, and most had a diameter of ~2 to 4 μm and a few had a diameter up to ~5 to 7 μm. A high-magnification SEM image, Fig. 2b, reveals that each flower is a hierarchical assembly of many interconnecting ultrathin (~2 to 5 nm thickness) and densely porous sheets. This suggests that after a thermal treatment no apparent collapses were observed and the original flower-like morphology of the intermediate was perfectly kept (Fig. S3†), except that there were numerous pores formed on the sheets. A high-magnification TEM image, Fig. 1c, further demonstrates that such an ultrathin sheet is full of a lot of pores with diameters of 10–50 nm (or Fig. S3d†). Such a pore with an area of *ca.* 180 nm^2 is shown by the HRTEM image, Fig. 2d. Actually, this sheet is a single-crystal with a highly crystalline structure, in which the structural uniformity is on an atomic scale and no amorphous materials were observed along the pore edge. The clearly resolved d-spacings of 0.24 nm and 0.21 nm correspond to the $\{1\bar{1}1\}$ and $\{002\}$ planes, respectively, of the cubic NiO crystal, respectively. Also shown is an FFT pattern (bottom-right inset in 2c) and which from this image can be indexed as the [110] zone axis of the NiO crystal. We further characterized Co_3O_4 in this material by means of the HRTEM image (Fig. S4†). The lattice fringes show the imaging characteristics of the spinel Co_3O_4 crystal, in which the d-spacing of 0.24 and 0.15 nm correspond to the distance of the $\{\bar{1}11\}$ and $\{02\bar{2}\}$ planes,

respectively, of the Co_3O_4 crystal. An inset in Fig. S4† is a fast Fourier transformation (FFT) pattern from this image, which can be indexed as the [211] zone axis of the Co_3O_4 crystal. The XRD pattern, Fig. S5d,† shows that these flower-like architectures are made up of the cubic phase NiO and spinel phase Co_3O_4. But, the composition of Co_3O_4 is lower than that of NiO in the composites. Energy-dispersive X-ray spectroscopy (EDX) elemental mappings, Fig. 2e, show that the Co, Ni and O elements uniformly distribute in the hybrid NiO/Co_3O_4 material. X-ray photoelectron spectroscopy (XPS) studies also determine the chemical composition of the composites, Fig. 2f (and Fig. S5†). A survey scan shows the presence of the three elements (Ni, Co and O) within the as-prepared hybrid NiO/Co_3O_4 material (clearly the C signal may be attributed to adventitious carbon). These results demonstrate that the as-prepared products were hybrid NiO/Co_3O_4 material with spherical flower-like architectures.

The other hybrid NiO/Co_3O_4 material shown in Fig. 3 was synthesized by using the mole ratio of 3 : 2 ($Ni(NO_3)_2$ to $Co(NO_3)_2$) and maintaining other synthetic conditions constant. As seen in a low-magnification SEM image, Fig. 3a, as-synthesized hybrid products are composed of a lot of uniform flower-like architectures with a mean diameter of ~1 μm. A high-magnification SEM image, Fig. 3b, shows that each flower is built from a considerable quantity of densely porous ultrathin sheets (~2 nm in thickness). These porous ultrathin sheets are interconnected forming a loose structure toward a common center. It means even through a thermal annealing the products well remain their original morphology (Fig. S6†), except that there are numerous pores formed on the sheets due to the release of the surfactant, H_2O, and gases from the sheets upon such an annealing process. A TEM image, Fig. 3c, clearly demonstrates that there are many pores with a diameter ~5 to 20 nm formed on this sheet (or Fig. S6d†). A HRTEM image taken from the edge of this sheet, Fig. 3d, demonstrates that this sheet is a single-crystal with a high crystallinity, in which the resolved d-spacing of 0.15 nm corresponds to the {02$\bar{2}$} planes of the NiO crystal. A bottom-left inset FFT pattern from this image in (c) can be indexed as the [111] zone axis of the NiO crystal. XRD pattern, Fig. S7,† conforms that these 3D flower-like architectures are composites composed of NiO and Co_3O_4 materials, which are also characterized by XPS spectra (Fig. S8†) and EDX elemental mappings (Fig. S9†). Taken the above together, two kinds of hybrid NiO/Co_3O_4 (4 : 1 and 3 : 2 of Ni to Co) materials with considerably different flower-like architectures are synthesized for their use as electrode materials.

These 3D hybrid NiO/Co_3O_4 flower-like architectures self-assembled by mesoporous and ultrathin nanosheets, which possess a large accessible surface area and interspaces, enable a synergistic effect of NiO and Co_3O_4 as individual constituents. These materials will provide the possibility of efficient transport of ions and electrons in the electrode, not only at the surfaces, but also throughout the bulk, and this is available more for a fast, reversible Faradic reaction during the charge storage process. As we know, differences of the pseudocapacitor materials' microstructures and compositions will result in a variation of the charge storage efficiency.[21] In our study, hybrid NiO/Co_3O_4 (4 : 1 and 3 : 2) flower-like architectures and comparative NiO flower-like architectures were all examined by cyclic voltammetry (CV) and galvanostatic charge–discharge (CD) measurements. The CV curves, Fig. 4a, were recorded from the hybrid NiO/Co_3O_4 (4 : 1) flower-like architectures at scan rates of 5, 10, 20, 50, 80 and 100 mV s^{-1} in a 1 M KOH aqueous solution. A couple of redox peaks were observed within the

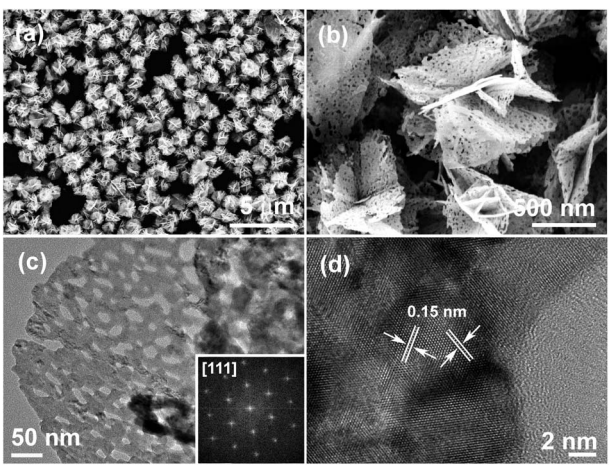

Fig. 3 (a and b) Low- and high-magnification SEM images of as-synthesized hybrid NiO/Co_3O_4 (3 : 2) materials. (c and d) TEM and HRTEM images, respectively, of an individual sheet, inset in (c) showing its corresponding FFT pattern.

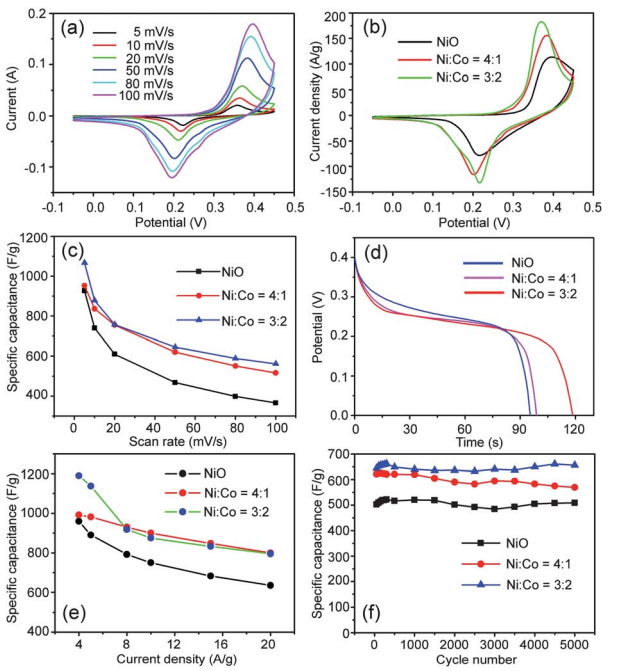

Fig. 4 (a) CV curves of the as-synthesized hybrid NiO/Co_3O_4 (4 : 1) architectures. (b) A comparison of the CV curves of the synthesized hybrid NiO/Co_3O_4 (4 : 1 and 3 : 2) and NiO architectures at a scan rate of 50 mV s^{-1}. (c) Specific capacitances of the as-synthesized materials at different scan rates. (d) A comparison of the specific capacitances of the synthesized materials at a current density of 4 A g^{-1}. (e) Specific capacitances of the synthesized materials at different current densities. (f) Cycling performance of the synthesized materials for 5000 cycles at a scan rate of 50 mV s^{-1}.

potential windows ranging from −0.05 to 0.45 V, and these peaks mainly resulted from redox reactions related to M–O/M–O–OH, where M represents Ni or Co ions.[22] Interestingly, with the scan rate increasing, the redox current increased. Also, the oxidation and reduction peaks shifted toward higher and lower potentials, respectively, with a large potential separation. These characteristics of the CV curves also demonstrated by the hybrid NiO/Co_3O_4 (3 : 2) flower-like architectures and the flower-like NiO architectures (Fig. S10†). The specific capacitances of two kinds of hybrid NiO/Co_3O_4 flower-like architectures and NiO flower-like architectures can be directly compared by their CV curves under the same scan rate, Fig. 4b. Obviously, the enclosed area of the second hybrid material is larger than that of the first hybrid material and the NiO architectures, indicating that the NiO/Co_3O_4 (3 : 2) flower-like architectures with a higher Co composition have a large specific capacitance. The specific capacitance of the electrodes is calculated from the CV curves according to the following equation $C = Q/m\Delta V$, where Q (C) is the average charge during the charging and discharging processes, m (g) is the mass of the active materials in the electrodes, and ΔV (V) is the potential window.[23] So, the specific capacitances of the three comparative materials were calculated based on their corresponding CV curves with different scan rates (Fig. 4a and Fig. S10†) and then plotted as a function of the scan rate, Fig. 4c. The specific capacitance of the second hybrid NiO/Co_3O_4 architectures (1068 F g^{-1}) was larger than that of the first one (953 F g^{-1}) and the NiO architectures (927 F g^{-1}) at a scan rate of 5 mV s^{-1}. When the scan rate increased to 100 mV s^{-1}, the specific capacitance of the two hybrid materials still remained at 516 and 562 F g^{-1}, respectively, displaying their good rate capability, while the specific capacitance of the NiO material was only 365 F g^{-1} at the same scan rate. Meanwhile, it can be seen that with the increase of the scan rate the specific capacitances of these electrode materials decreased. This may be attributed to the argument that a high scan rate prevents the accessibility of ions from entering into all the pores within the electrode materials, and thus the transport of ions is limited (due to their slow diffusion) and only the outer surface can be utilized for the charge storage.[9a] Such an improved electrochemical performance of the hybrid NiO/Co_3O_4 architectures was further confirmed by CD tests performed at different current densities. The discharge specific capacitance was calculated from the discharge curves using the following equation: $C = It/m\Delta V$, where I (A) is the current density used for the charge/discharge, t (s) is the discharge time, m (g) is the weight of the active electrode and ΔV (V) is the voltage interval of the discharge.[23] The specific capacitances of the three comparative materials were calculated based on their corresponding discharge curves at different current densities. At a current density of 4 A g^{-1}, a direct comparison of their discharge curves is shown in Fig. 4d. Here, the specific capacitance of the second hybrid material (1190 F g^{-1}) is larger than that of the first one (992 F g^{-1}) and the NiO architectures (960 F g^{-1}). As we know, a high discharge rate or a high current density is of great importance for the real devices that involve a fast charging–discharging process.[24] So, it should examine the specific capacitances of the three comparative materials at a varying current density with a maximum value of 20 A g^{-1}. Based on the discharge curves of the three kinds of as-synthesized materials (Fig. S11†), the summary plots of the specific capacitance *vs.* the current density are shown in Fig. 4e. To our surprise, with an increase of the charging–discharging rate from 4 to 20 A g^{-1}, the hybrid NiO/Co_3O_4 (4 : 1) material only shows a ∼19% specific capacitance loss (from 992 to 804 F g^{-1}), which is much lower than that of the hybrid NiO/Co_3O_4 (3 : 2) material (∼33%) and the NiO architectures (∼34%), respectively, revealing their good rate capability, as confirmed earlier by the CV. Such an excellent rate capability may be attributed to a short ion diffusion path within the interesting architectures assembled by many interconnecting ultrathin and dense and porous sheets (Fig. 2) as well as a strong synergistic effect between NiO and Co_3O_4 materials with the right composition combination.

Cycling performance is another key factor in determining the applicability of supercapacitors for many practical applications, with an excellent cycling stability being crucial for real supercapacitor operations. In this study, a long-term cycle stability of the as-synthesized products as an electrode material was evaluated by repeating the CV test at a scan rate of 50 mV s^{-1} for 5000 cycles, Fig. 4f. It can be clearly seen that the specific capacitances of three such kinds of electrode material gradually increased at first and then slightly decreased. This indicates that there is an activation process of the electrode at the beginning period of the CV cycling test.[21a,23] During this process, the electrode will be completely activated through the intercalation and de-intercalation of ions through some circulations, resulting in the increase of active points inside the electrode materials, hence enhancing the specific capacitance. During the first 300 cycles, the specific capacitance of the NiO architectures increases from 502 to 522 F g^{-1}, while in the first 150 cycles, the specific capacitance for the hybrid NiO/Co_3O_4 (4 : 1) architectures increased from 622 to 624 F g^{-1}. After 5000 cycles, the specific capacitance of the two materials could retain 97.5% (∼509 F g^{-1}) and 92.3% (∼576 F g^{-1}) of their maximum capacitances, respectively. Comparatively, the specific capacitance of the hybrid NiO/Co_3O_4 (3 : 2) architectures increased from 644 to 662 F g^{-1} after the initial 300 cycles, and then remained at 99.1% of the maximum capacitance (∼656 F g^{-1}) after 5000 cycles, suggesting a very steady behavior during these CV cycling tests. Notably, the electrolytes of the three electrode materials remained transparent even after 5000 cycling tests, indicating a minimal dissolution of active material into the solution, which can be attributed to their excellent cycle stability as active electrode materials.

The specific capacitance and rate capability of the as-synthesized hybrid NiO/Co_3O_4 (4 : 1 and 3 : 2) electrode materials are better than that of the prepared NiO electrode material and to the best of our knowledge, such good electrochemical performances of these hybrid materials are also better than the reported NiO- and Co_3O_4-based electrode materials, particularly at a high scan rate.[8b,15,16,18,25] These good performances can be mainly attributed to the morphological characteristics of the mesoporous and ultrathin nanosheets self-assembling into flower-like architectures, as well as the rational composition of the two constituents (NiO and Co_3O_4).

Clearly, mesoporous and ultrathin nanosheets within the 3D architectures can provide more active sites for efficient electrolyte ions transportation, not only at the active materials surface but also throughout the bulk. These microstructure characteristics were analyzed by means of Brunauer–Emmett–Teller (BET, surface areas of 36.2, 56.9 and 53.9 $m^2 g^{-1}$ for the three as-prepared materials, respectively) and Barrett–Joyner–Halenda (BJH, average pore sizes of 12.1, 24.3 and 17.3 nm, respectively) (Fig. S12†). Moreover, the open and free interspaces both among these nanosheets and inside the pores on the nanosheets can act as an "ion reservoir" that can shorten the diffusion distance from the external electrolyte to the interior surfaces and thus minimize ion transport resistance, which will significantly enhance the intercalation/deintercalation of ions and improve the utilization rate of electrode materials even at high rates.[26] Compared with the NiO materials, the hybrid NiO/Co_3O_4 materials with a rational composition not only fully utilize individual constituents effectively, resulting from increasing the number of active sites, but also have a strong synergistic effect between NiO and Co_3O_4 materials, thus showing excellent performances in terms of both specific capacitance and rate capability.

4 Conclusions

In summary, a facile, environmentally friendly, and low-cost synthetic method resulted in a large-scale synthesis of 3D mesoporous hybrid NiO/Co_3O_4 flower-like architectures for high-performance supercapacitors. These architectures not only have mesoporous and ultrathin nanosheets self-assembled with considerable interspaces, providing more active sites for efficient electrolyte ions transportation at the active materials surface and throughout the bulk, but also show a strong synergistic effect between NiO and Co_3O_4 constituents with a rational composition. The hybrid NiO/Co_3O_4 flower-like architectures demonstrate excellent electrochemical performances in supercapacitors, such as large specific capacitances, excellent rate capability and long-term cycle stability. These remarkable electrochemical properties, as well as many advantages associated with the synthetic method (such as simplicity, high yield and low-cost), should make the present hybrid NiO/Co_3O_4 flower-like architectures a competitive electrode material for next generation supercapacitors.

Acknowledgements

This work was financially supported by the National Natural Science Foundation of China (Grant no. 21171035), the Science and Technology Commission of Shanghai-based "Innovation Action Plan" Project (Grant no. 10JC1400100), Ph.D. Programs Foundation of Ministry of Education of China (Grant no. 20110075110008), Key Grant Project of Chinese Ministry of Education (Grant no. 313015), Shanghai Rising-Star Program (Grant no. 11QA1400100), Fundamental Research Funds for the Central Universities, the Shanghai Leading Academic Discipline Project (Grant no. B603), and the Program of Introducing Talents of Discipline to Universities (Grant no. 111-2-04).

Notes and references

1 (*a*) D. R. Rolison, J. W. Long, J. C. Lytle, A. E. Fischer, C. P. Rhodes, T. M. McEvoy, M. E. Bourga and A. M. Lubersa, *Chem. Soc. Rev.*, 2009, **38**, 226; (*b*) H. G. Zhang, X. D. Yu and P. V. Braun, *Nat. Nanotechnol.*, 2011, **6**, 277.

2 S. F. Leung, M. Yu, Q. F. Lin, K. Kwon, K. L. Ching, L. L. Gu, K. Yu and Z. Y. Fan, *Nano Lett.*, 2012, **12**, 3682.

3 (*a*) R. de la Rica and H. Matsui, *Chem. Soc. Rev.*, 2010, **39**, 3499; (*b*) P. Kaur, Y. Maeda, A. C. Mutter, T. Matsunaga, Y. J. Xu and H. Matsui, *Angew. Chem., Int. Ed.*, 2010, **49**, 8375.

4 (*a*) L. L. Zhang, Z. G. Xiong and X. S. Zhao, *ACS Nano*, 2010, **4**, 7030; (*b*) R. J. Zou, Z. Y. Zhang, L. Yu, Q. W. Tian, Z. G. Chen and J. Q. Hu, *Chem.–Eur. J.*, 2011, **17**, 13912.

5 (*a*) J. R. Miller and P. Simon, *Science*, 2008, **321**, 651; (*b*) P. Simon and Y. Gogotsi, *Nat. Mater.*, 2008, **7**, 845; (*c*) C. Liu, F. Li, L. P. Ma and H. M. Cheng, *Adv. Mater.*, 2010, **22**, 28; (*d*) G. P. Wang, L. Zhang and J. J. Zhang, *Chem. Soc. Rev.*, 2012, **41**, 797.

6 (*a*) Z. J. Fan, J. Yan, L. J. Zhi, Q. Zhang, T. Wei, J. Feng, M. L. Zhang, W. Z. Qian and F. Wei, *Adv. Mater.*, 2010, **22**, 3723; (*b*) Y. Huang, J. J. Liang and Y. S. Chen, *Small*, 2012, **22**, 1805.

7 (*a*) C. C. Hu, K. H. Chang, M. C. Lin and Y. T. Wu, *Nano Lett.*, 2006, **6**, 2690; (*b*) J. T. Zhang, J. Z. Ma, L. L. Zhang, P. Z. Guo, J. W. Jiang and X. S. Zhao, *J. Phys. Chem. C*, 2010, **114**, 13609.

8 (*a*) J. H. Kim, K. Zhu, Y. F. Yan, C. L. Perkins and A. J. Frank, *Nano Lett.*, 2010, **10**, 4099; (*b*) C. Y. Cao, W. Guo, Z. M. Cui, W. G. Song and W. Cai, *J. Mater. Chem.*, 2011, **21**, 3204; (*c*) B. Wang, J. S. Chen, Z. Y. Wang, S. Madhavi and X. W. Lou, *Adv. Energy Mater.*, 2012, **2**, 1188.

9 (*a*) R. B. Rakhi, W. Chen, D. Cha and H. N. Alshareef, *Nano Lett.*, 2012, **12**, 2559; (*b*) C. Z. Yuan, L. Yang, L. R. Hou, L. F. Shen, X. G. Zhang and X. W. Lou, *Energy Environ. Sci.*, 2012, **5**, 7883.

10 (*a*) W. Y. Li, Q. Liu, Y. G. Sun, J. Q. Sun, R. J. Zou, G. Li, X. H. Hu, G. S. Song, G. X. Ma, J. M. Yang, Z. G. Chen and J. Q. Hu, *J. Mater. Chem.*, 2012, **22**, 14864; (*b*) G. H. Yu, L. B. Hu, M. Vosgueritchian, H. L. Wang, X. Xie, J. R. McDonough, X. Cui, Y. Cui and Z. N. Bao, *Nano Lett.*, 2011, **11**, 2905.

11 (*a*) S. D. Perera, B. Patel, N. Nijem, K. Roodenko, O. Seitz, J. P. Ferraris, Y. J. Chabal and K. J. Balkus, *Adv. Energy Mater.*, 2011, **1**, 936; (*b*) J. Benson, S. Boukhalfa, A. Magasinski, A. Kvit and G. Yushin, *ACS Nano*, 2012, **6**, 118.

12 (*a*) S. Ghosh and O. Inganäs, *Adv. Mater.*, 1999, **11**, 1214; (*b*) L. Nyholm, G. Nyström, A. Mihranyan and M. Strømme, *Adv. Mater.*, 2011, **23**, 3751; (*c*) G. H. Yu, L. B. Hu, N. Liu, H. L. Wang, M. Vosgueritchian, Y. Yang, Y. Cui and Z. N. Bao, *Nano Lett.*, 2011, **11**, 4438.

13 R. B. Rakhi, W. Chen, D. K. Cha and H. N. Alshareef, *J. Mater. Chem.*, 2011, **21**, 16197.

14 (*a*) K. W. Nam and K. B. Kim, *J. Electrochem. Soc.*, 2002, **149**, A346; (*b*) X. X. Qing, S. Q. Liu, K. L. Huang, K. Z. Lv, Y. P. Yang, Z. G. Lu, D. Fang and X. X. Liang, *Electrochim. Acta*, 2011, **56**, 4985.

15 C. Z. Yuan, X. G. Zhang, L. H. Su, B. Gao and L. F. Shen, *J. Mater. Chem.*, 2009, **19**, 5772.

16 S. K. Meher and G. R. Rao, *J. Phys. Chem. C*, 2011, **115**, 15646.
17 (*a*) J. P. Liu, J. Jiang, C. W. Cheng, H. X. Li, J. X. Zhang, H. Gong and H. J. Fan, *Adv. Mater.*, 2011, **23**, 2076; (*b*) L. Q. Mai, F. Yang, Y. L. Zhao, X. Xu, L. Xu and Y. Z. Luo, *Nat. Commun.*, 2012, **2**, 381.
18 X. H. Xia, J. P. Tu, Y. Q. Zhang, X. L. Wang, C. D. Gu, X. B. Zhao and H. J. Fan, *ACS Nano*, 2012, **6**, 5531.
19 C. Guan, X. L. Li, Z. L. Wang, X. H. Cao, C. Soci, H. Zhang and H. J. Fan, *Adv. Mater.*, 2012, **24**, 4186.
20 J. H. Zhong, A. L. Wang, G. R. Li, J. W. Wang, Y. N. Ou and Y. X. Tong, *J. Mater. Chem.*, 2012, **22**, 5656.
21 (*a*) X. H. Lu, D. Z. Zheng, T. Zhai, Z. Q. Liu, Y. Y. Huang, S. Xiea and Y. X. Tong, *Energy Environ. Sci.*, 2011, **4**, 2915; (*b*) M. K. Song, S. Cheng, H. Y. Chen, W. T. Qin, K. W. Nam, S. C. Xu, X. Q. Yang, A. Bongiorno, J. Lee, J. M. Bai, T. A. Tyson, J. Cho and M. L. Liu, *Nano Lett.*, 2012, **12**, 3483.
22 H. L. Wang, Q. M. Gao and L. Jiang, *Small*, 2011, **7**, 2454.
23 J. Yan, E. Khoo, A. Sumboja and P. S. Lee, *ACS Nano*, 2010, **4**, 4247.
24 Z. G. Yang, J. L. Zhang, M. C. W. Kintner-Meyer, X. C. Lu, D. W. Choi, J. P. Lemmon and J. Liu, *Chem. Rev.*, 2011, **111**, 3577.
25 (*a*) X. H. Xia, J. P. Tu, Y. J. Mai, X. L. Wang, C. D. Gu and X. B. Zhao, *J. Mater. Chem.*, 2011, **21**, 9319; (*b*) Y. H. Xiao, S. J. Liu, F. Li, A. Q. Zhang, J. H. Zhao, S. M. Fang and D. Z. Jia, *Adv. Funct. Mater.*, 2012, **22**, 4052; (*c*) J. P. Liu, J. Jiang, M. Bosmanc and H. J. Fan, *J. Mater. Chem.*, 2012, **22**, 2419; (*d*) X. H. Xia, J. P. Tu, Y. Q. Zhang, Y. J. Mai, X. L. Wang, C. D. Gu and X. B. Zhao, *RSC Adv.*, 2012, **2**, 1835.
26 (*a*) D. W. Wang, F. Li, M. Liu, G. Q. Lu and H. M. Cheng, *Angew. Chem., Int. Ed.*, 2008, **47**, 373; (*b*) X. Y. Lang, A. Hirata, T. Fujita and M. W. Chen, *Nat. Nanotechnol.*, 2011, **6**, 232.